IEEE Access
Multidisciplinary | Rapid Review | Open Access Journal

Received September 21, 2021, accepted October 9, 2021, date of publication October 18, 2021, date of current version October 26, 2021.

*Digital Object Identifier 10.1109/ACCESS.2021.3121019*

# Combinative Voltage Vector-Based Model Predictive Control for Performance Improvement of Quasi Z-Source Inverter

**YUHAO XU AND HAIFENG XIAO**
School of Electronics Engineering, Xi'an Aeronautical University, Xi'an 710077, China
Corresponding author: Yuhao Xu (xyuh7006@126.com)

This work was supported in part by the Natural Science Foundation of Shaanxi Province, China, under Grant 2020JM-632; and in part by the Natural Science Foundation of Shaanxi Provincial Department of Education, China, under Grant 21JC014.

**ABSTRACT** Model predictive control (MPC) has been commonly recognized as a promising control strategy for the quasi Z-source inverter (qZSI). However, large control error is regarded as an innate drawback of MPC due to only one voltage vector applied per control cycle. In this paper, an improved MPC, namely combinative voltage vectors based MPC, is proposed for the qZSI to reduce the control error and improve steady-state performance. Two different voltage vectors are applied in one control cycle, so that the cost function value can be reduced. The errors of the inductor current, the capacitor voltage, and the output current of the qZSI included in the cost function can be decreased greatly. Furthermore, the performance investigation of the proposed method indicates that the two selected voltage vectors consisting of a non-shoot-through vector and a shoot-through vector is of help in shorting the charge-discharge period of inductor. Thus, the inductor current ripple as well as the total harmonics distortion (THD) of the output current is greatly reduced. The experimental results show the validity and the advantages of the proposed method.

**INDEX TERMS** Quasi Z-source inverter, model predictive control, cost function, weighting factor.

## I. INTRODUCTION

In 2002, a new type of dc-ac converter called Z-source inverter (ZSI) was proposed by Peng [1], which has attracted widespread concern of scholars. The buck-boost function of ZSI is achieved using the Z-source network and employing the shoot-through (ST) state. Therefore, the bridge arm in the same phase can be short-circuited, improving the security and reliability of the inverter [2], [3]. The dead time is also not required. The quasi Z-source inverter (qZSI) was proposed as an improved or alternative version of the ZSI. The input current of the dc source is continuous in the ST state and the capacitor voltage stress of the quasi Z-source network is reduced [4]. Hence, the qZSI is considered to have broad application prospects in the field of new energy [5], [6], such as driving system of electric vehicle and photovoltaic system.

The linear control technique is regarded as an efficient way to control the qZSI. The direct and the indirect dc-link voltage control methods are developed as the two classical strategies for the qZSI [7], [8]. Despite achieving satisfactory performance, simultaneous control of dc-side and ac-side of the qZSI makes the cascaded control loops very complicated [9]. Moreover, the characteristic of nonminimum phase is exhibited on the dc-side [10]. To solve this problem, a challenging task, reducing the effect of nonminimum phase on the qZSI to the lowest degree, need to be completed.

With the rapid development of the powerful microprocessors, model predictive control (MPC) has gained much attention in the fields of power electronics and motor drives [11]-[16]. Particularly, finite control set MPC (FCS-MPC) has been extensively studied, for its merits of fast response, simple control structure, and easy to handle the nonlinearity for the controlled variables. Thus, FCS-MPC is going to be an effective method with high dynamic performance for the qZSI [17], [18].

According to the principle of FCS-MPC, the future value of the inductor current, the capacitor voltage, and the output current of the qZSI under different voltage vectors are predicted and then incorporated into a cost function for obtaining the optimal voltage vector [19]. This control scheme is also

The associate editor coordinating the review of this manuscript and approving it for publication was Yonghao Gui.

known as the conventional MPC for the qZSI, which discards the modulator for obtaining high dynamic performance [20]. However, the time of control period has significant influence on the performance of the conventional MPC over that of other control methods for the qZSI. Due to only one voltage vector applied over the whole control cycle, large control error is caused at long control cycle [21]–[23]. Although it is a feasible way for the reduction of the control error, shortening the control cycle has limited effect because of heavy calculation burden in MPC.

Recently, a few research works have been published to change the connatural characteristics of the conventional MPC, and thereby overcoming the aforementioned problem. A variable switching point predictive current control was proposed for the qZSI in [24]. The switches position can be changed at any time instant within the sampling interval for reducing the output and inductor currents ripples. A direct model predictive current control strategy for the qZSI is proposed in [25]. The controlled variables are predicted within a long horizon, so that the strategy can see more future information about the system behavior. It has been proved that the strategy can effectively reduce the THD of the output current. In [26], a logical operation-based model predictive control is proposed for the qZSI to improve the control accuracy of the inductor current. By using control logic, the inductor current is separated from the cost function for independent control. Through setting an error reference of the inductor current, the inductor current is allowed to change only within its error reference. Hence, a small inductor current ripple is obtained. In [27], a predictive control with an integral action aimed at eliminating the steady-state error was proposed when confronted with low switching frequencies. By employing just one integral, the proposed strategy is able to compensate for the steady-state error in both ac and dc variables without impacting the dynamic response.

In this paper, a combinative voltage vector based MPC is proposed to reduce the control error and improve steady-state performance of the qZSI. In the proposed method, two different voltage vectors are selected from eight candidate voltage vectors and applied in one control cycle. The selection of the first voltage vector is the same as the optimal voltage vector selection in the conventional MPC. The first voltage vector is switched to the second one at right time in the control cycle. The selection of the second voltage vector and the working time of the two voltage vectors are carefully calculated to guarantee that the cost function value under the two selected voltage vectors are lower than that under one optimal voltage vector. Therefore, the control error of the qZSI can be greatly reduced because it is incorporated into the cost function. The performance analysis for the qZSI shows that the inductor current ripple and the THD of the output current have significant decrease at a long control cycle. Therefore, the steady-state performance of the qZSI is overall improved. Experimental results verify the validity and the advantages of the proposed method. The contribution of the proposed method can be summarized as follows:

1) A multi voltage vector MPC is developed to the qZSI, achieving the performance improvement of the qZSI. Lower inductor current ripple, capacitor voltage ripple, and output current THD can be obtained.

2) Low inductor current ripple obtained by the proposed method indicates that small inductor can be used in the qZSI, and thus the volume and the cost of the qZSI can be reduced.

3) The output power quality of the qZSI is improved, since the proposed method has lower output current THD than the conventional MPC.

## II. PREDICTION MODEL OF QZSI

The qZSI consists of a dc voltage source, a quasi Z-source network, a three-phase inverter, and a *RL* load, as shown in Fig.1. The dc source voltage is boosted to the desired dc-link voltage through the quasi Z-source network. By using the active and null vectors, the desired output voltage vector can be obtained. The boosting feature of the qZSI is implemented through adding an extra ST vector. Thus, there are totally eight space voltage vectors applied for the qZSI, seven vectors in the non-ST state and one vector in the ST state.

When the space vector modulation (SVM) based method, namely voltage and current dual close-loop control strategy, is applied to the qZSI, the capacitor voltage and the inductor current are taken as the controlled variable of outer loop and inner loop, respectively, while the three-phase output currents are controlled by the conventional current closed loop method. Hence, the three loops make the qZSI control system very complicated.

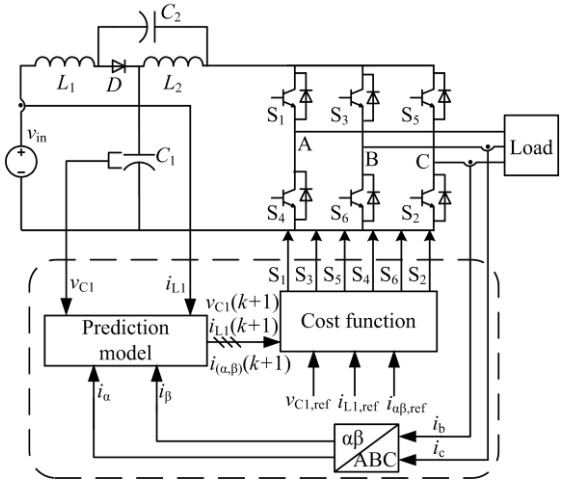


**FIGURE 1.** QZSI topology.

When MPC is applied to the qZSI, the control structure of system has a greatly simplification. As shown in Fig. 1, the current of the inductor $L_1$ ($i_{L1}$), the voltage of the capacitor $C_1$ ($v_{C1}$), and the three output currents ($i_a$, $i_b$, and $i_c$) converted into $\alpha\beta$ axis currents ($i_\alpha$ and $i_\beta$) at current moment are firstly sampled for their state prediction at next moment. Secondly, the predicted values $v_{C1}(k+1)$, $i_{L1}(k+1)$, and $i_{\alpha\beta}(k+1)$, and the reference commands $v_{C1,ref}$, $i_{L1,ref}$, and $i_{\alpha\beta,ref}$, are sent into the cost function to obtain an optimal

voltage vector. Finally, the optimal voltage vector is transformed into the inverter switching state to control the qZSI.

### A. PREDICTIVE OUTPUT CURRENT

The output voltage $v_{out}$ can be expressed as

$$v_{out} = 2v_{dc}(S_1 + aS_3 + a^2S_5)/3 \tag{1}$$

where $v_{dc}$ is dc-link voltage, and $a = 1/2+j\sqrt{3}/2$. Assuming the output of the qZSI is connected to three-phase $RL$ load, the output voltage balance equation is given by

$$v_{out} = L\frac{di_{(\alpha,\beta)}}{dt} + Ri_{(\alpha,\beta)} \tag{2}$$

where $i_\alpha$ and $i_\beta$ are components of three-phase output currents in $\alpha\beta$ coordinate system; $R$ and $L$ are resistance and the inductance of $RL$ load.

According to Euler method, the differential of the output current can be expressed by the following discrete-time model

$$\frac{di_{(\alpha,\beta)}(k)}{dt} = \frac{i_{(\alpha,\beta)}(k) - i_{(\alpha,\beta)}(k - T_s)}{T_s} \tag{3}$$

where $k$, $k$-$T_s$, and $T_s$ represent present moment, last moment, and control period, respectively. The time is shifted forward one step to obtain the future value of the output current, which is expressed as follows

$$i_{(\alpha,\beta)}(k + T_s) = [T_s v_{out}(k + T_s) + Li_{(\alpha,\beta)}(k)]/(RT_s + L) \tag{4}$$

### B. PREDICTIVE INDUCTOR CURRENT AND CAPACITOR VOLTAGE

The equivalent circuit of the qZSI is shown in Fig. 2. Different in the ST and non-ST states, the predictive models of the capacitor voltage and the inductor current should be derived separately.

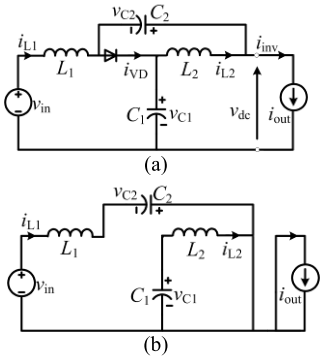


**FIGURE 2.** Equivalent circuits of qZSI in (a) non-ST state and (b) ST state.

#### 1) NON-ST STATE

As shown in Fig. 2(a), when the qZSI works in the non-ST state (including null state and active state), the current of the inductor $L_1$ and the voltage of the capacitor $C_1$ can be expressed as follows

$$i_{L1} = i_{inv} + C_1\frac{dv_{C1}}{dt} \tag{5}$$

$$v_{C1} = v_{in} - L_1\frac{di_{L1}}{dt} \tag{6}$$

where $C_1$ and $L_1$ are the capacitance and the inductance of the quasi Z-source network, respectively; $v_{in}$ and $v_{C1}$ are the voltages of the dc source and the capacitor $C_1$, respectively; $i_{L1}$ is the current of the inductor $L_1$; $i_{inv}$ is the output current of the quasi Z-source network, which can be solved by the following switching state function

$$i_{inv} = S_1 i_a + S_3 i_b + S_5 i_c \tag{7}$$

In (7), $i_a$, $i_b$, and $i_c$ are the three-phase output currents. It is important to note that $i_{inv}$ is zero when the qZSI operates in the null state. By using Euler method to discrete (5) and (6), the predictive inductor current and capacitor voltage are derived as

$$i_{L1}(k + T_s) = T_s[v_{in} - v_{C1}(k)]/L_1 + i_{L1}(k) \tag{8}$$

$$v_{C1}(k + T_s) = T_s[i_{L1}(k + T_s) - i_{inv}(k + T_s)]/C_1 + v_{C1}(k) \tag{9}$$

#### 2) ST STATE

Fig. 2(b) shows the equivalent circuits of the qZSI in the ST state. According to the principle of the qZSI [4], the inductors $L_1$ and $L_2$ with the same inductance have the same current and voltage. Thus, the current and voltage of the inductor $L_2$ can be replaced by those of the inductor $L_1$, which are given as

$$L_1\frac{di_{L1}}{dt} = v_{C1} \tag{10}$$

$$C_1\frac{dv_{C1}}{dt} = -i_{L1} \tag{11}$$

To calculate the predictive inductor current and capacitor voltage in the ST state, (10) and (11) are discretized as

$$i_{L1}(k + T_s) = T_s v_{C1}(k)/L_1 + i_{L1}(k) \tag{12}$$

$$v_{C1}(k + T_s) = -T_s i_{L1}(k + T_s)/C_1 + v_{C1}(k) \tag{13}$$

## III. COMBINATIVE VOLTAGE VECTORS BASED MODEL PREDICTIVE CONTROL FOR QUASI Z-SOURCE INVERTER

To reduce control error and improve the steady-state performance of the qZSI, an improved MPC method, namely combinative voltage vectors based MPC, is proposed in this paper. In this section, the principle of the proposed method is first given in part A. The realization, the control structure, and the performance analysis of the proposed method are presented in part B, C, and D, respectively.

### A. PRINCIPLE OF PROPOSED METHOD

In the conventional MPC, only one voltage vector that has the minimal cost function value among the eight candidate voltage vectors is applied in the whole control cycle. In the proposed method, two voltage vectors are selected from the

eight candidate voltage vectors and applied in one control cycle, making sure that the cost function value is lower than that under the conventional MPC. The reduction of the cost function value is of benefit to the decrease of the control error of the qZSI, for the reason that the errors between the references values and the predictive values of controlled variables are included in the cost function.

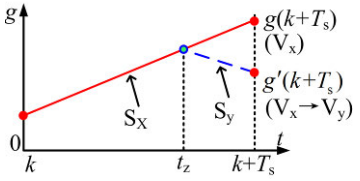


**FIGURE 3.** Principle of switching voltage vector.

The principle of the proposed method is illustrated by an example, as shown in Fig. 3. Under the optimal voltage vector $V_x$, the cost function value follows the path $S_x$ and equals $g(k + T_s)$ at the moment $k + T_s$. If two voltage vectors are applied in the control cycle, the first voltage vector $V_x$ is able to switched to the second one $V_y$ at the moment $t_z$. Therefore, under $V_x$ and $V_y$, the cost function follows the path $S_x$ from the moment $k$ to $t_z$ and the path $S_y$ from the moment $t_z$ to $k + T_s$. The cost function value becomes $g'(k + T_s)$ at $k + T_s$ moment. By using the two voltage vectors, the cost function value can be decreased from $g(k + T_s)$ to $g'(k + T_s)$. That means the errors of the inductor current, the capacitor voltage, and the output current included in the cost function are reduced.

### B. IMPLEMENTATION OF PROPOSED METHOD

The key points in the implementation of the proposed method are the selection of the first and second voltage vectors and the calculation of the working time of the two voltage vectors, which are completed by the following three steps.

#### 1) FIRST VOLTAGE VECTOR SELECTION

In the first step, the aim is to select the first voltage vector by the cost function. The realization is the same as that in the conventional MPC. The cost function is given as follows

$$g = \lambda_i[i_{\alpha,\mathrm{ref}} - i_\alpha(k + T_s)]^2 + \lambda_i[i_{\beta,\mathrm{ref}} - i_\beta(k + T_s)]^2 + \lambda_C[v_{C1,\mathrm{ref}} - v_{C1}(k+T_s)]^2 + \lambda_L[i_{L1,\mathrm{ref}} - i_{L1}(k+T_s)]^2 \tag{14}$$

where $\lambda_i$, $\lambda_C$, and $\lambda_L$ are the weighting factors of the output current, the capacitor voltage, and the inductor current, respectively. $i_{\alpha,\mathrm{ref}}$, $i_{\beta,\mathrm{ref}}$, $v_{C1,\mathrm{ref}}$, and $i_{L1,\mathrm{ref}}$ are the references of the output currents on $\alpha$ and $\beta$ coordinate axes, the capacitor voltage, and the inductor current, respectively. Since the inductor current, the capacitor voltage, and the output current are the three controlled variables with different physical nature, they have different importance to the qZSI control system. To balance the performance of the three controlled variables and stabilize the qZSI control system, several weighting factors should be properly selected for the cost function. The errors between these references and predictive values under different voltage vectors are evaluated by the cost function for choosing the first voltage vector that has the minimal cost function value.

#### 2) SWITCHING TIME INSTANT OF VOLTAGE VECTOR

In the second step, the aim is to calculate the switching time instant of the first voltage vector and the second one. Supposing $V_1$ is the first voltage vector selected by the cost function in step 1, $V_2 \sim V_8$ can be used as the candidate voltage vectors of the second voltage vector. Therefore, the switching time instants of these candidate voltage vectors need to be calculated.

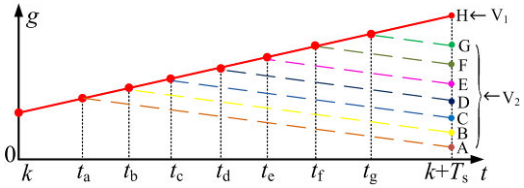


**FIGURE 4.** Change in cost function value when voltage vector V1 is switched to V2.

The calculation of switching time instant of the voltage vectors $V_1$ and $V_2$ can be illustrated by Fig. 4. It can be seen that the cost function value at $k + T_s$ moment is H due to applying $V_1$ over the whole control cycle. Using two voltage vectors $V_1$ and $V_2$ switched at the time instant $t_a \sim t_g$ in one control cycle, the cost function can be changed from H to A∼G. Naturally, the possible switching time of the two voltage vectors can be a value between 0 and $T_s$, but only $t_a \sim t_g$ are given in Fig. 4 for the convenience of description. Among all the possible switching time instant, the one that make the cost function have minimum value at $k+T_s$ moment is selected. The calculation process of switching time instant is given follows as.

The slopes of inductor current, capacitor voltage, and output current under voltage vectors $V_1$ and $V_2$ are obtained by

$$\begin{cases} k_{L1} = [i^1_{L1}(k + T_s) - i_{L1}(k)]/T_s \\ k_{C1} = [v^1_{C1}(k + T_s) - v_{C1}(k)]/T_s \\ k_{a1} = [i^1_\alpha(k + T_s) - i_\alpha(k)]/T_s \\ k_{b1} = [i^1_\beta(k + T_s) - i_\beta(k)]/T_s \end{cases} \tag{15}$$

$$\begin{cases} k_{L2} = [i^2_{L1}(k + T_s) - i_{L1}(k)]/T_s \\ k_{C2} = [v^2_{C1}(k + T_s) - v_{C1}(k)]/T_s \\ k_{a2} = [i^2_\alpha(k + T_s) - i_\alpha(k)]/T_s \\ k_{b2} = [i^2_\beta(k + T_s) - i_\beta(k)]/T_s \end{cases} \tag{16}$$

In (15) and (16), $k_{L1}$, $k_{C1}$, $k_{a1}$, and $k_{b1}$ are slopes of the inductor current, capacitor voltage, and output current respectively under voltage vector $V_1$, respectively; $k_{L2}$, $k_{C2}$, $k_{a2}$, and $k_{b2}$ are the slopes of the inductor current, capacitor voltage, and output current respectively under the voltage vector $V_2$, respectively. By (15) and (16), the predictive inductor current,

capacitor voltage, and output current are

$$\begin{cases} i'_\alpha(k+T_s) = i_\alpha(k) + k_{a1}t_1 + k_{a2}(T_s - t_1) \\ i'_\beta(k+T_s) = i_\beta(k) + k_{b1}t_1 + k_{b2}(T_s - t_1) \\ v'_{C1}(k+T_s) = v_{C1}(k) + k_{C1}t_1 + k_{C2}(T_s - t_1) \\ i'_{L1}(k+T_s) = i_{L1}(k) + k_{L1}t_1 + k_{L2}(T_s - t_1) \end{cases} \tag{17}$$

where $t_1$ is switching time instant of voltage vector. To calculate $t_1$, the predictive values in (17) are substituted into the cost function expressed by

$$\begin{aligned} g_1 = {} & \lambda_i[i_{\alpha,\text{ref}} - i'_\alpha(k+T_s)]^2 + \lambda_i[i_{\beta,\text{ref}} - i'_\beta(k+T_s)]^2 \\ & + \lambda_C[v_{C1,\text{ref}} - v'_{C1}(k+T_s)]^2 + \lambda_L[i_{L1,\text{ref}} - i'_{L1}(k+T_s)]^2 \end{aligned} \tag{18}$$

In (18), as $g_1$ is the function of $t_1$, $t_1$ can be derived by minimizing $g_1$. This is done by setting the derivative of $g_1$ equal to zero.

$$\frac{dg_1}{dt_1} = 0 \tag{19}$$

This yields

$$t_1 = -(m+n)/z \tag{20}$$

where

$$\begin{cases} m = \lambda_C(k_{C1} - k_{C2})(k_{C2}T_s + v_{C1}(k) - v_{C1,\text{ref}}) \\ \quad + \lambda_L(k_{L1} - k_{L2})(k_{L2}T_s + i_{L1}(k) - i_{L1,\text{ref}}) \\ n = \lambda_i(k_{a1} - k_{a2})(k_{a2}T_s + i_\alpha(k) - i_{\alpha,\text{ref}}) \\ \quad + \lambda_i(k_{b1} - k_{b2})(k_{b2}T_s + i_\beta(k) - i_{\beta,\text{ref}}) \\ z = [\lambda_i(k_{a1} - k_{a2})^2 + \lambda_i(k_{b1} - k_{b2})^2 \\ \quad + \lambda_C(k_{C1} - k_{C2})^2 + \lambda_L(k_{L1} - k_{L2})^2] \end{cases}$$

Having known the switching time instant of $V_1$ and $V_2$, the switching time instants that $V_1$ is switched to $V_3$~$V_8$ can be calculated using the same algorithm above.

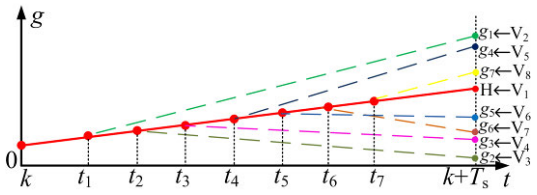


**FIGURE 5.** Change in cost function value when voltage vector V1 is switched to V2~V8.

### 3) SECOND VOLTAGE VECTOR SELECTION

In the third step, the purpose is to select the second voltage vector among the seven candidate voltage vectors $V_2$~$V_8$. As shown in Fig. 5, the cost function value becomes $g_1 \sim g_7$ at $k+T_s$ when $V_1$ is switched to $V_2$~$V_8$ at the switching time instants $t_1 \sim t_7$ obtained in step 2. $g_1 \sim g_7$ are compared to obtain the minimum one expressed by

$$g_x(t_z) = \min[g_1(t_1), g_2(t_2), \ldots, g_7(t_7)] \tag{21}$$

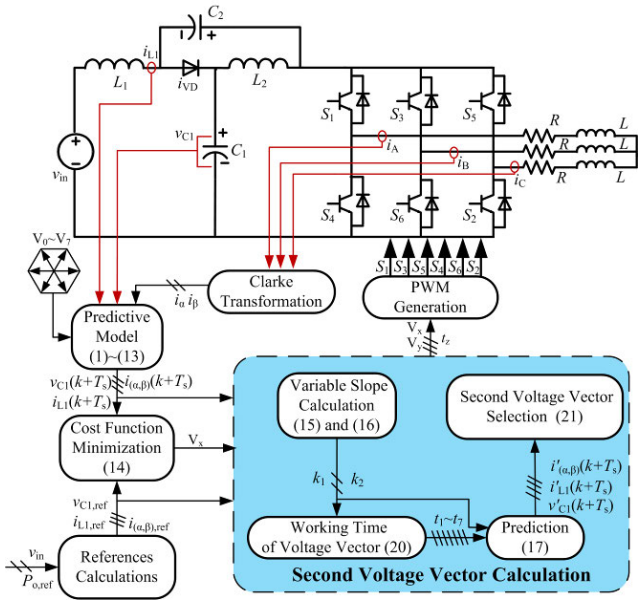


**FIGURE 6.** System structure diagram of the proposed method for qZSI.

According to (21), the voltage vector that has the minimal cost function value is chosen as the second vector. The first and second voltage vectors can be selected in steps 1 and 3 while the switching time instant of the two vectors can be calculated in step 2. Finally, the selected voltage vectors will be converted to PWM signal for the qZSI control.

### C. CONTROL SYSTEM BLOCK DIAGRAM

The system structure diagram of the proposed method is shown in Fig. 6. The block diagram is divided into three parts, the reference calculation, the model prediction, and the voltage vector selection. The references of the inductor current, the capacitor voltage, and the output current are calculated in the reference calculation module according to the dc source voltage and the desired output power. The future values of the inductor current, capacitor voltage, and output current are predicted in the model predictive module. All the references and the predictive values are sent into the cost function to obtain the first voltage vector $V_x$. The second voltage vector $V_y$ and the switching time instant $t_z$ are calculated in the second vector calculation module. The PWM generation module outputs PWM signals to control the qZSI according to $V_x$, $V_y$ and $t_z$. The main difference between the proposed method and the conventional MPC is that the proposed method contains the second vector calculation and the PWM generation modules, which generate two different switching states in one control cycle.

### D. PERFORMANCE ANALYSIS

By using the proposed method, the cost function value is smaller than that of the conventional MPC. The cost function consists of the sum of the errors between the predictive values and the reference values of the inductor current, the capacitor voltage, and the output current, so the reduction of the value

of the cost function makes the predictive values approximate to the reference values. By this way, the control error of the controlled variable can be reduced. Therefore, lower inductor current ripple, capacitor voltage ripple, and output current THD are obtained. The volume and the cost of the qZSI topology can be decreased. Furthermore, the output power quality is improved.

### 1) INDUCTOR CURRENT

In the steady-state, the average inductor current is almost unchanged, and the charging and discharging inductor current ripples are equal according to the principle of volt-second balance. Hence, when two voltage vectors are applied in the control cycle, one of them must be ST vector causing the inductor to charge, and the other must be non-ST vector causing the inductor to discharge. The operation time of the two voltage vectors should guarantee the charging inductor current ripple equals to the discharging inductor current ripple, and thus achieving the minimization of the inductor current ripple. Fig. 7 shows the inductor current waveforms under the proposed method and the conventional MPC. In Fig. 7(a), the ST and non-ST vectors under the proposed method are applied during $t_1 \sim t_2$ and $t_2 \sim t_3$, respectively, so the discharging and charging of the inductor can be finished in one control cycle. However, the ST vector is applied over the whole control cycle under the conventional MPC, as shown in Fig. 7(b). Therefore, the non-ST vector must be applied for at least one control cycle or more to balance the charging inductor current ripple.

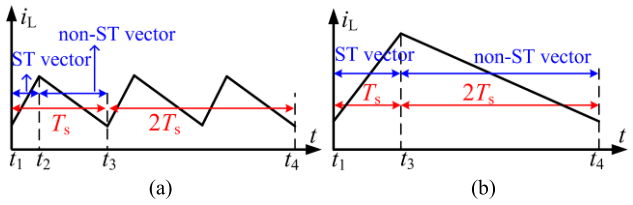


**FIGURE 7.** Inductor current waveforms of (a) proposed method and (b) conventional MPC.

It can be found from Fig. 7 that the inductor current ripple of the proposed method is lower than that of the conventional MPC due to the increased charging and discharging frequency of the inductor. To compare the current ripples of the two methods, the maximum inductor current ripple must be calculated first. Since the volt-second balance principle is satisfied, either charging current ripple or discharge one can represent the maximum current ripple. Taking it as an example, the charging current ripple can be expressed as

$$\Delta i_{\mathrm{Lsh}} = (v_{\mathrm{dc}} + v_{\mathrm{in}})T_{\mathrm{sh}}/L_1 \tag{22}$$

where $T_{\mathrm{sh}}$ is the shoot-through time. It should be noted that $T_{\mathrm{sh}}$ is different in the conventional MPC and the proposed method. $T_{\mathrm{sh}}$ is equal to the control cycle time $T_{\mathrm{s}}$ in the conventional MPC, as only one voltage vector is applied per control cycle.

Through replacing $T_{\mathrm{sh}}$ by $T_{\mathrm{s}}$, the inductor current ripple of the conventional MPC $\Delta i_{\mathrm{Lnsh-MPC}}$ is obtained as

$$\Delta i_{\mathrm{Lsh\text{-}MPC}} = (v_{\mathrm{dc}} + v_{\mathrm{in}})T_{\mathrm{s}}/2L_1 \tag{23}$$

In the proposed method, the variable $T_{\mathrm{sh}}$ is shorter than $T_{\mathrm{s}}$. It is necessary to first solve the $T_{\mathrm{sh}}$ by associating the equations of charging and discharging current ripples. According to (6), the discharging inductor current ripple of the propose method $\Delta i_{\mathrm{Lnsh-DVMPC}}$ can be expressed as

$$\Delta i_{\mathrm{Lnsh\text{-}DVMPC}} = (v_{\mathrm{dc}} - v_{\mathrm{in}})(T_{\mathrm{s}} - T_{\mathrm{sh}})/2L_1 \tag{24}$$

Solved from (24) and (22), $T_{\mathrm{sh}}$ is given as

$$T_{\mathrm{sh}} = (v_{\mathrm{dc}} - v_{\mathrm{in}})T_{\mathrm{s}}/2v_{\mathrm{dc}} \tag{25}$$

By substituting (25) into (22), the inductor current ripple of the proposed method $\Delta i_{\mathrm{Lsh-DVMPC}}$ is derived as

$$\Delta i_{\mathrm{Lsh\text{-}DVMPC}} = (v_{\mathrm{dc}} + v_{\mathrm{in}})(v_{\mathrm{dc}} - v_{\mathrm{in}})T_{\mathrm{s}}/v_{\mathrm{dc}}/4L_1 \tag{26}$$

By using the simulation parameters, the inductor current ripples of proposed method and conventional MPC under different dc-link voltages expressed by (23) and (26)are pictured in Fig. 8. The inductor current ripples of the two methods increases with the dc-link voltage. However, the inductor current ripple of the proposed method is much smaller than that of the conventional MPC. From Fig. 7, it can be seen that the inductor current ripple of the proposed method is between 0.1A and 0.75A while in the conventional MPC is between 2.1A and 3A. Therefore, the proposed method can effectively reduce the inductor current ripple, especially under low dc-link voltage gain.

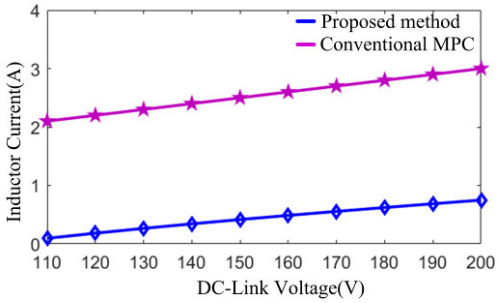


**FIGURE 8.** Inductor current ripples of proposed method and conventional MPC under different dc-link voltages.

### 2) CAPACITOR VOLTAGE AND OUTPUT CURRENT

The charging and discharging law of the capacitor is the same as that of the inductor. The non-ST time and ST time are all reduced in the proposed method, so the ripple of the capacitor voltage will be reduced.

The output current is influenced by the inductor current ripple because the inductor current ripple is superimposed on the output current. Thus, the inductor current ripple reduction is helpful to reduce the output current ripple and the THD of the output current.

## IV. SIMULATION AND EXPERIMENTAL RESULTS

In this section, the performance of the proposed method is compared with that of the conventional MPC by simulation and experiment to verify the advantage of the proposed method in reduction of control error.

### A. SIMULATION RESULT

A three-phase two-level qZSI with RL load is built in MATLAB/Simulink with the parameters listed in TABLE 1. The weighting factors $\lambda_L$, $\lambda_i$, and $\lambda_C$ are tuned by using the trial and error method [17]. Based on large numbers of experimental tests, $\lambda_L$, $\lambda_i$, and $\lambda_C$ in the proposed method and the conventional MPC are finally set as 6, 2, and 1, respectively. The steady-state and dynamic performance of the qZSI using the proposed method and the conventional MPC are investigated in the simulation. The results are shown in Figs. 9 and 10.

**TABLE 1. Simulation parameters.**

| Parameter | Value |
|---|---|
| DC source voltage $v_{in}$ | 100V |
| Inductance of $L_1$ and $L_2$ | 4 mH |
| Capacitance of $C_1$ and $C_2$ | 560 $\mu$F |
| Load resistance | 10 $\Omega$ |
| Load inductance | 7.7 mH |
| Control period | 80 $\mu$s |

In the steady-state simulation, the peak dc-link voltage boosted by the qZSI is twice the dc source voltage under the output power of 950W. Figs. 9 and 10 show simulation results of the proposed method and the conventional MPC in the steady-state, respectively. The dc-link voltage is boosted to 200V in the non-ST state and decreases to 0V in the ST state. The capacitor voltage and the peak output current remain around 150V and 8A, respectively. The inductor current fluctuates near its reference 9.5A. It is concluded that the inductor current, the output current, the capacitor voltage, and the dc-link voltage of the qZSI can follow their reference commands with accuracy and rapidity by using the two methods. Therefore, the qZSI obtains a stable performance. Nevertheless, the tracking behaviors of the qZSI under the proposed method and the conventional MPC indicate their different performance in control error. The inductor current ripple of the proposed method is 0.9A, three tenths that of the conventional MPC 3A. The capacitor voltage ripple of the proposed method is 0.5V, two thirds that of the conventional MPC 1.5V. Furthermore, it is clearly observed that the output current ripple of the proposed method is also lower than that of the conventional MPC. Therefore, the proposed method exhibits a good performance in control of current and voltage ripples.

In the dynamic simulation, the peak dc-link voltage is stepped up from 150V to 200V, and thus the output power is changed from 520W to 950W. Figs. 11 and 12 show the dynamic response waveforms of the proposed method and the conventional MPC. The output currents of the two methods are different in the dynamic process. The output current of the proposed method is sinusoidal in the transient process, and its amplitude increases with the amplitude of the dc-link voltage. However, the output current of conventional MPC is seriously

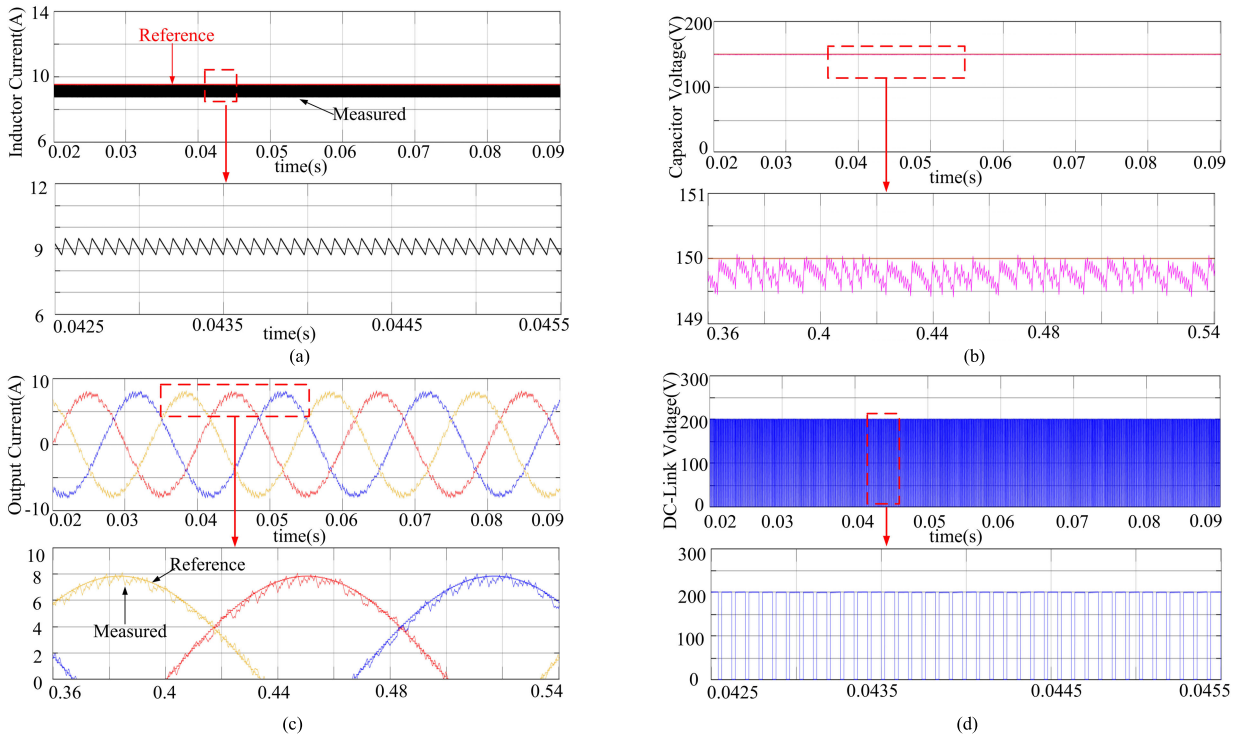


**FIGURE 9. Simulation results of proposed method of (a) inductor current, (b) capacitor voltage, (c) output current, and (d) dc-link voltage in the steady-state.**

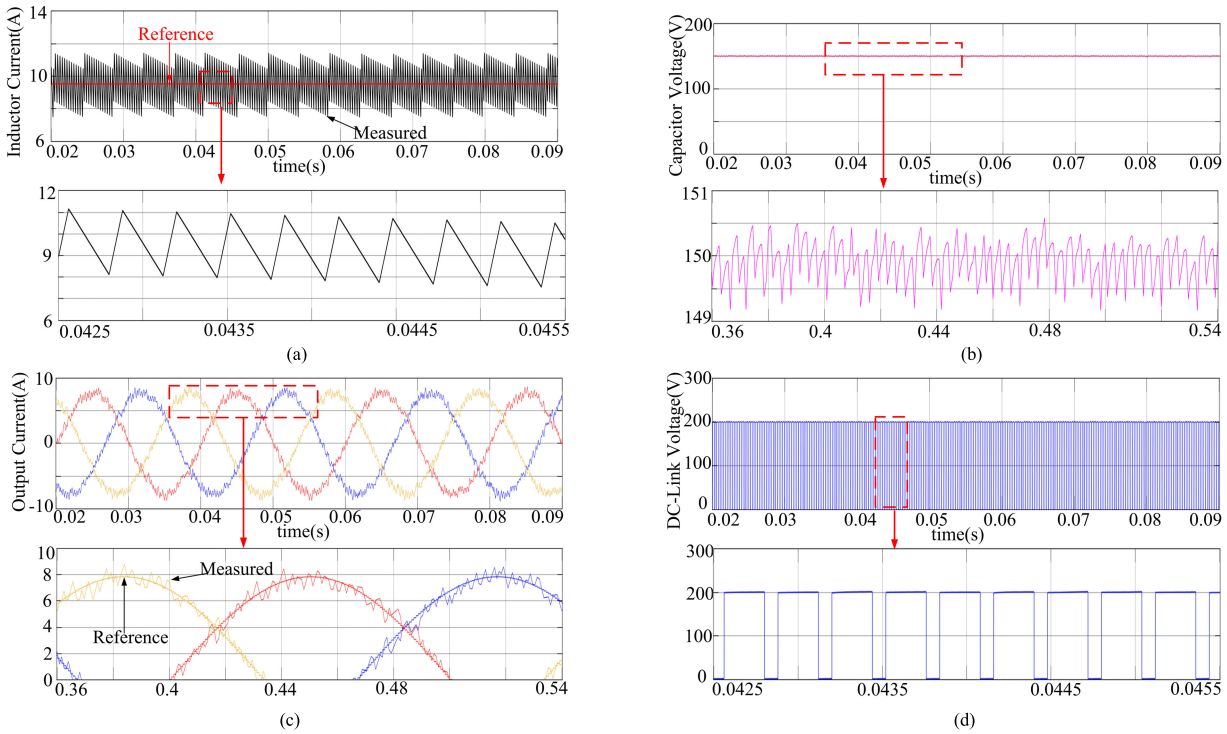


**FIGURE 10.** Simulation results of conventional MPC of (a) inductor current, (b) capacitor voltage, (c) output current, and (d) dc-link voltage in the steady-state.

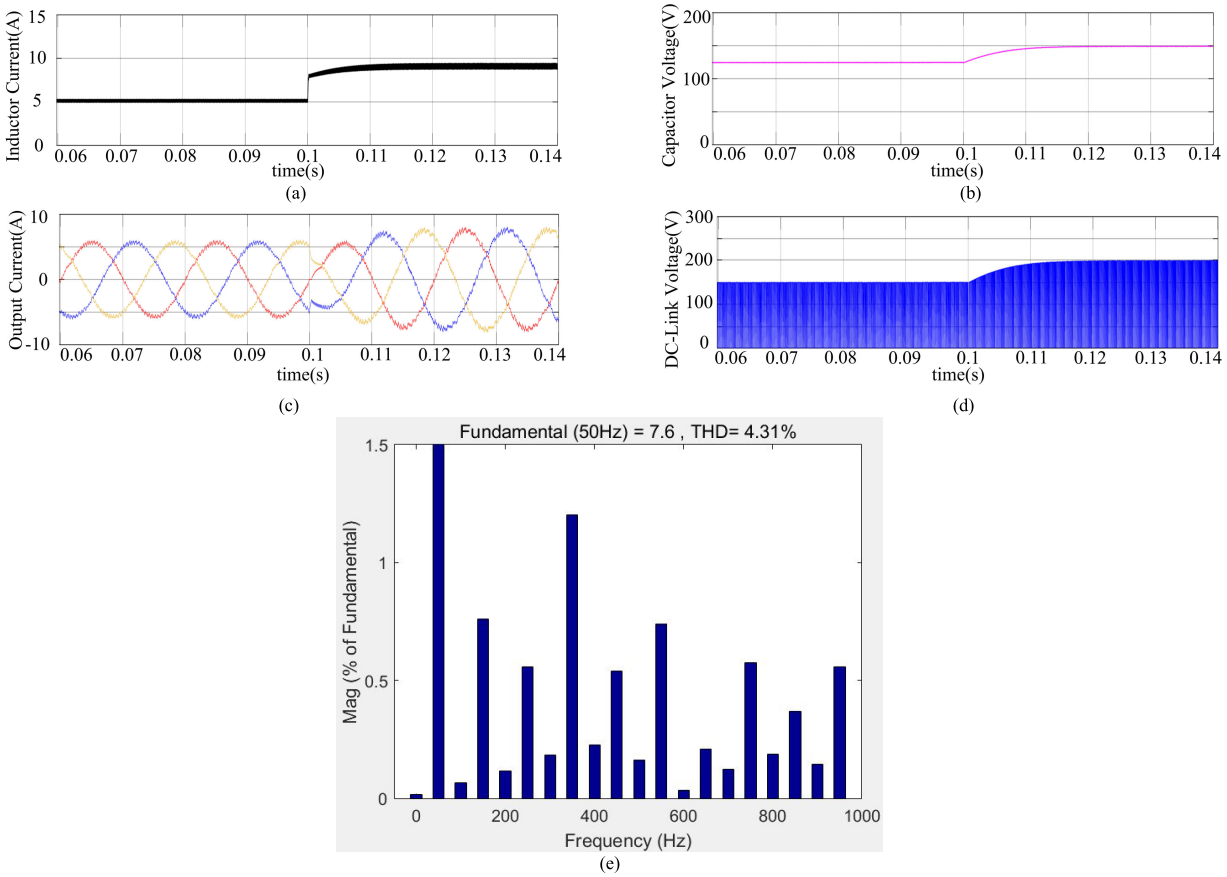


**FIGURE 11.** Dynamic response of proposed method of (a) inductor current, (b) capacitor voltage, (c) output current, (d) dc-link voltage, and (e) harmonics spectrum.

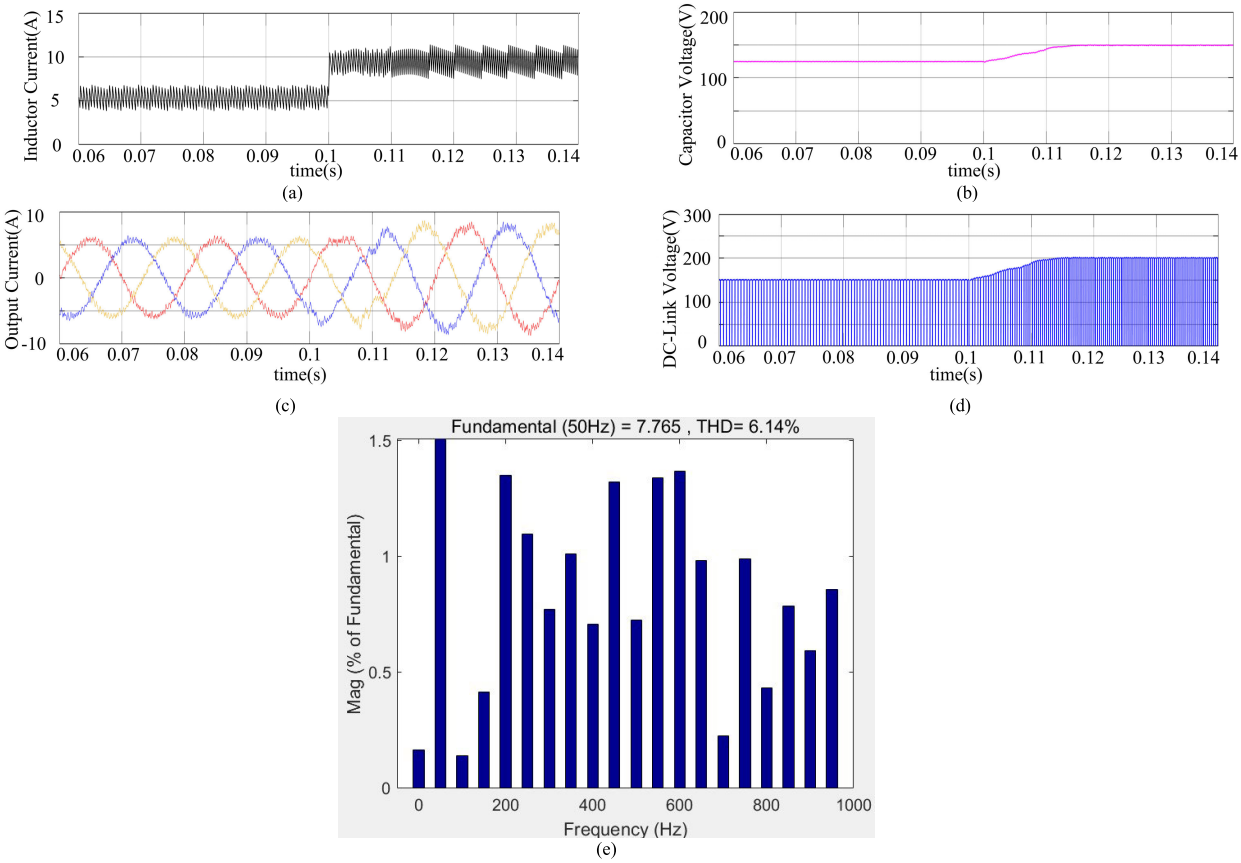


**FIGURE 12.** Dynamic response of conventional MPC of (a) inductor current, (b) capacitor voltage, (c) output current, (d) dc-link voltage, and (e) harmonics spectrum.

distorted in the transient process. Moreover, it is tested that the output current THD of the proposed method is 4.31% lower than that of the conventional MPC 6.14%. From the waveforms of the capacitor voltage and the dc-link voltage, it is seen that the qZSI completes a smooth transition using the proposed method. The simulation results validate that the proposed method exhibits dynamic performance better than the conventional MPC.

### B. EXPERIMENTAL RESULT

A three-phase qZSI setup was built to verify the performance of proposed method experimentally, as shown in Fig. 13. The digital signal processor TMS320F28335 is main controller, generating six driven signals for the switch devices of the power circuit. The proposed algorithm is programmed according to Fig. 6. The system parameters are the same as the simulation ones. The steady-state and dynamic experiment results are given as follows.

#### 1) STEADY-STATE EXPERIMENT

In order to obtain satisfactory control performance for the proposed method and the conventional MPC in the experiment, it is necessary to obtain proper weighting factors from lots of experiment tests. Therefore, the experiments for getting the reasonable weighting factor are made under a safe

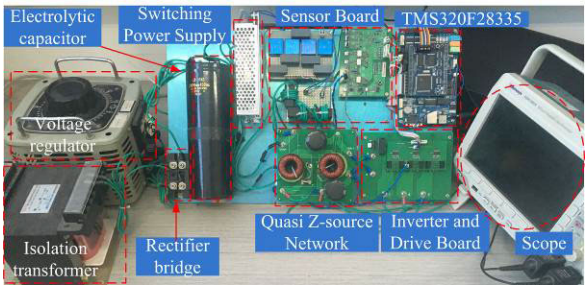


**FIGURE 13.** Three-phase qZSI experimental platform.

voltage limitation. $P_o^*$ is 120W, and $v_{dc}$ and $v_{in}$ are set to 100V and 50V, respectively. Therefore, $i_{L1}^*$, $i_{(\alpha,\beta)}^*$, and $v_{C1}^*$ are calculated as 2.4A, 2.78A, and 75V, respectively.

Fig. 14 shows the experiment results of the conventional MPC under different weighting factors. The tuning work of the weighting factors is done by fixing $\lambda_C$ and adjusting $\lambda_L$ and $\lambda_i$. Firstly, in Fig. 14(a), the capacitor voltage, the dc-link voltage, and the output current can achieve desired performance when $\lambda_L$, $\lambda_C$, and $\lambda_i$ are set as 6, 1.2, and 1, respectively. Secondly, the control performance of the inductor current becomes deteriorated when $\lambda_L$ is decreased to 3 or $\lambda_i$ is increased to 2, as shown in Fig. 14(b). The maximum inductor current ripple increases to 4.8A. If $\lambda_L$ is further

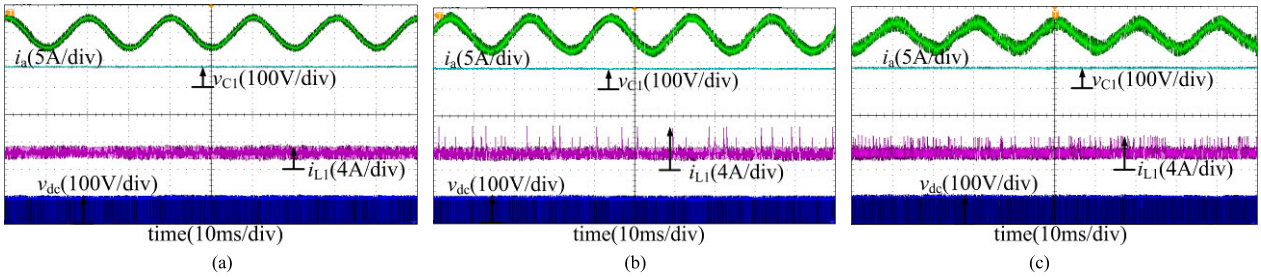


**FIGURE 14.** Experiment results of tuning weighting factors. (a) Conventional MPC with $\lambda_L = 6$, $\lambda_C = 1.2$, and $\lambda_i = 1$. (b) Conventional MPC with $\lambda_L = 3$, $\lambda_C = 1.2$, and $\lambda_i = 1$. (c) Conventional MPC with $\lambda_L = 9$, $\lambda_C = 1.2$, and $\lambda_i = 1$.

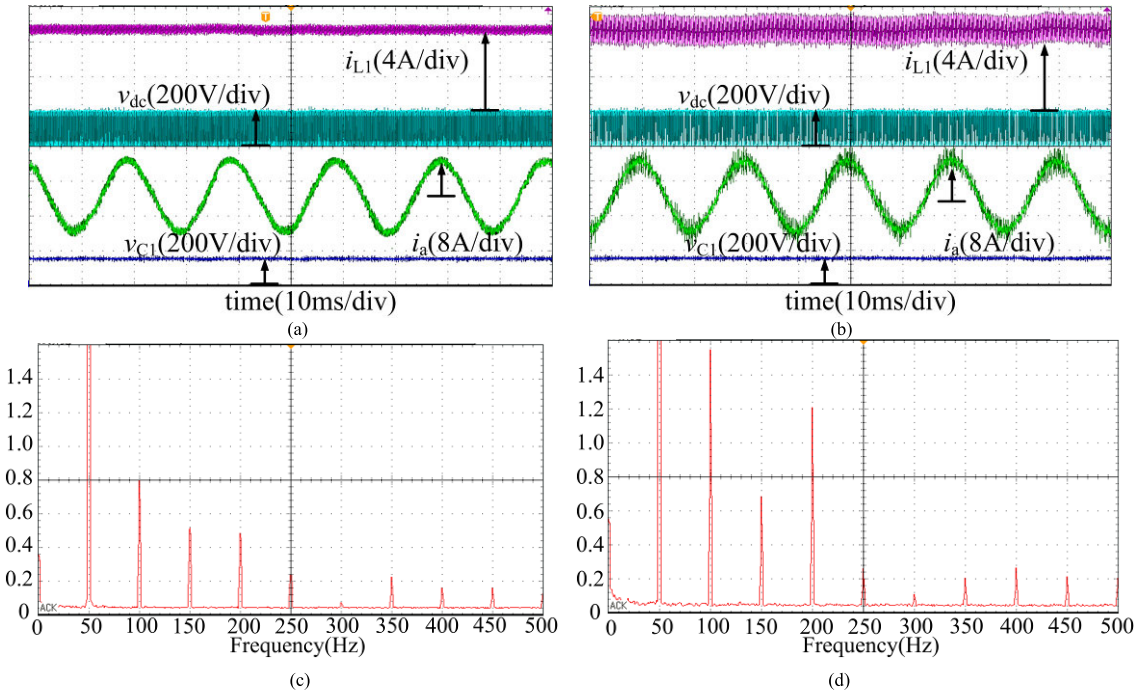


**FIGURE 15.** Steady-state experiment results. (a) $i_{L1}$, $v_{dc}$, $v_{C1}$, and $i_a$ of proposed method. (b) $i_{L1}$, $v_{dc}$, $v_{C1}$, and $i_a$ of conventional MPC. (c) Harmonic spectrum of output current of proposed method. (d) Harmonic spectrum of output current of conventional MPC.

decreased or $\lambda_i$ is further increased, the control system will be instable. Thirdly, the output current is distorted when $\lambda_L$ is increased to 9 or $\lambda_i$ is decreased to 0.6, as shown in Fig. 14(c). If $\lambda_L$ is further increased or $\lambda_i$ is further decreased, the output current will become worse. Therefore, the best control performance of the conventional MPC is achieved under the condition that $\lambda_L$, $\lambda_C$, and $\lambda_i$ are 6, 1.2, and 1, which are used in the following experiment.

To maintain the dc-link voltage at a constant value 200V, the capacitor voltage is controlled at 150V in the steady-state. The reference commands of output current and inductor current under the output power of 950W are kept as 7.9A and 9.5A, respectively, according to the power conservation. Fig. 15 shows the results of the steady-state experiment. The proposed method and the conventional method can ensure that the values of the controlled variables of the qZSI are stable near their reference values. However, the difference of the two methods in control performance is also clearly seen. As two voltage vectors applied in one control cycle, the proposed method has higher switching frequency than the conventional method. Therefore, the enveloping curves of the output current and the inductor current of the proposed method are much thinner than those of the conventional MPC. In Figs. 15 (a) and (b), the inductor current ripple of the proposed method is 0.8A lower than that of conventional MPC 3.1A. In Figs. 15 (c) and (d), the second, third, fourth, and fifth harmonics of the output current of the proposed method are 0.76%, 0.48%, 0.44%, and 0.2%, respectively, while they are 1.52%, 0.64%, 1.16%, and 0.2% in the conventional MPC, respectively. The output current THD is calculated as 4.8% in the proposed method lower than that in the conventional MPC 7.1%.

### 2) DYNAMIC EXPERIMENT

To investigate the dynamic performance of the proposed method, the output power is stepped down from 950W to 450W at the peak dc-link voltage $v_{dc}$ of 200V, achieving 75.9% power decrease. The experiment results are displayed in Figs. 16 and 17. Influenced by the change of the output

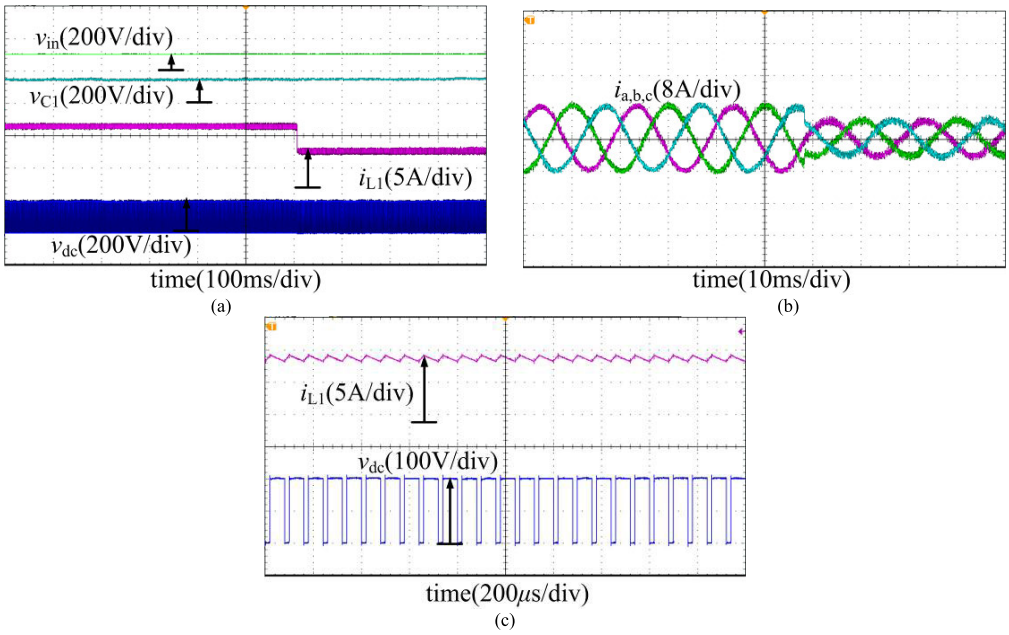


**FIGURE 16.** Dynamic experiment results of proposed method. (a) Capacitor voltage, inductor current, and dc-link voltage. (b) Three-phase output current. (c) Zoomed-in view of dc-link voltage and inductor current.

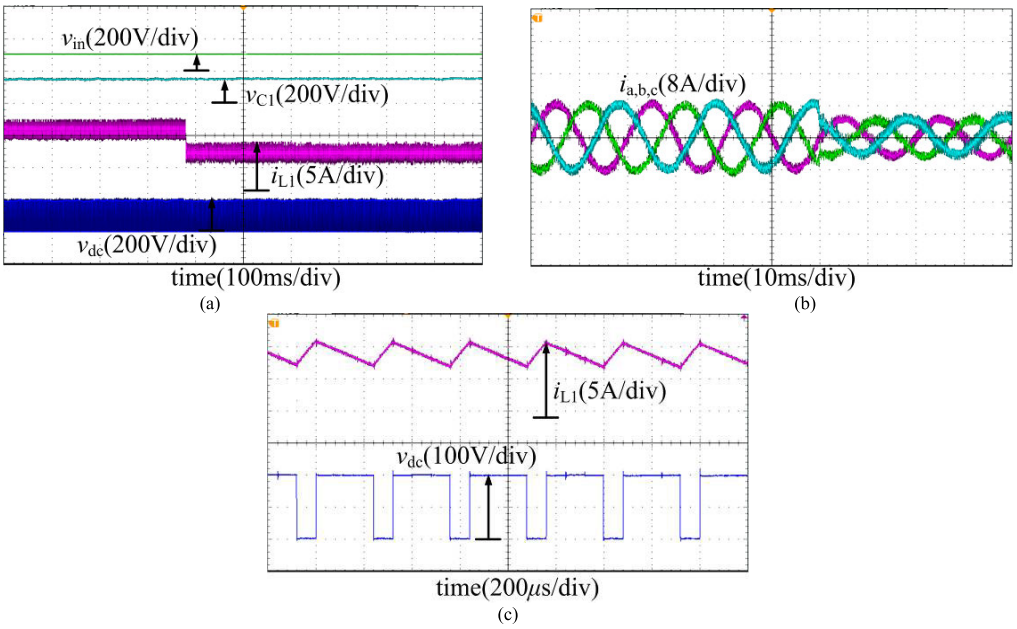


**FIGURE 17.** Dynamic experiment results of conventional MPC. (a) Capacitor voltage, inductor current, and dc-link voltage. (b) Three-phase output current. (c) Zoomed-in view of dc-link voltage and inductor current.

power, the average inductor currents of the two methods in the dynamic process all increase from 5.3A to 9.5A, the peak output currents from 5.8A to 7.9A, and the capacitor voltages is kept as 150V. From the zoomed-in view at the dc-link voltage of 200V, it can be seen that the ST time and the non-ST time using the proposed method are 20$\mu$s and 60$\mu$s respectively while using the conventional MPC are 80$\mu$s and 240$\mu$s respectively. Affected by the ST and non-ST time, the inductor $L_1$ has a charge-discharge cycle of 80$\mu$s in the proposed method shorter than that in the conventional MPC 320$\mu$s. Moreover, the inductor current ripple of the proposed method is 0.8A at dc-link voltage of 200V, only 0.267 times that of the conventional MPC 3A. Particularly, the output current of the conventional MPC has a large output current ripple at the peak, leading to a sinusoidal waveform distortion. By comparison, the proposed method can effectively reduce the output current ripple with the help of applying double vectors. The experimental results verify that the proposed method can achieve good dynamic performance as well as steady-state performance improvement on control error.

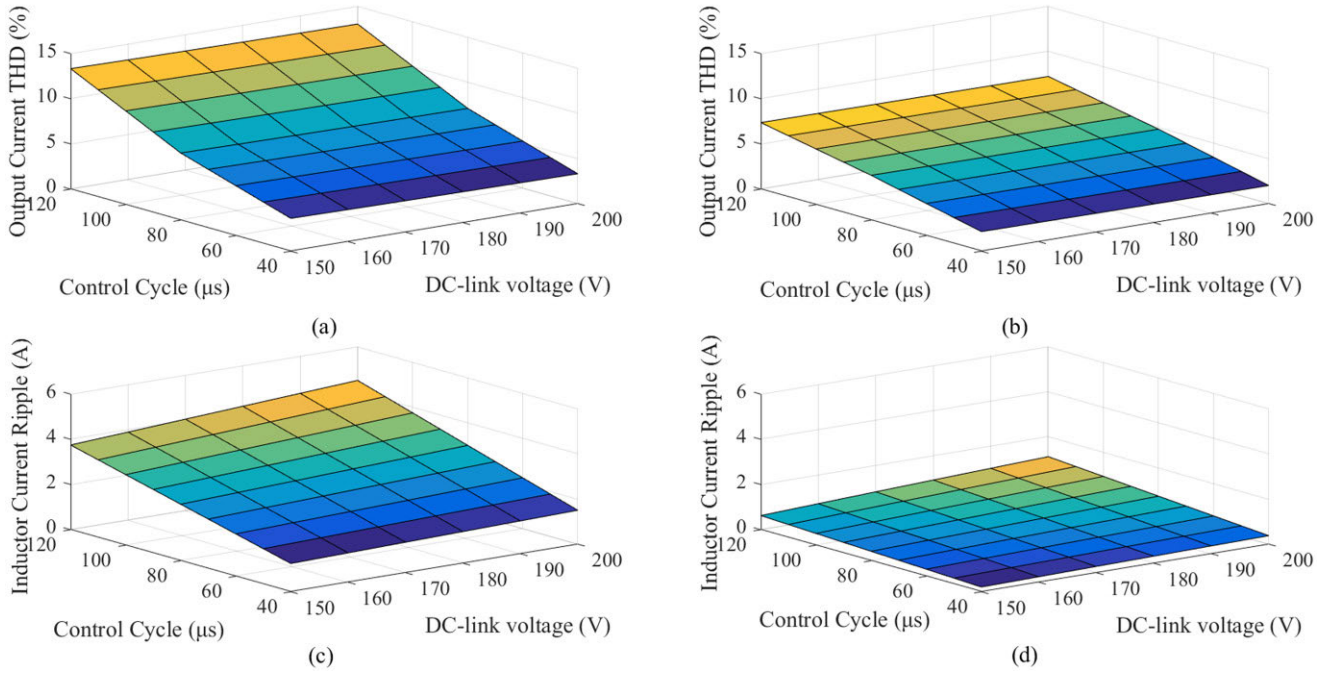


**FIGURE 18.** Experiment results under different control cycle and dc-link voltage. (a) Output Current THD of Conventional MPC. (b) Output Current THD of proposed method. (c) Inductor current ripple of Conventional MPC. (d) Inductor current ripple of proposed method.

In order to further study the performance improvement effect of the proposed method for the qZSI, the experiments are carried out under different control cycle and dc-link voltage. The experimental results are concluded in Fig. 18. It can be seen from Figs. 18 (a) and (b) that the THD of the output current of the two methods is mainly affected by the control cycle rather than the dc-link voltage. The longer the control cycle is, the larger the THD is. From the control cycle of 40$\mu$s to 120$\mu$s, the output current THD of the conventional MPC changes from 3.9% to 13%, while that of the proposed method from 2% to 7.2%. In Figs. 18 (c) and (d), the inductor current ripples of the two methods increase with the control cycle and the dc-link voltage. However, the conventional MPC is great influenced by the two factors over the proposed method. When the control cycle is 120 $\mu$s, the inductor current ripple of the conventional MPC is about 4.5A with the change of dc-link voltage, while that of the proposed method can maintain less than 1.1A in the whole region. It should be worthy noted from Fig. 18 that the inductor current ripple of the proposed method is 1/4 that of the conventional MPC when the dc-link voltage gain is 200V and the control cycle is 120$\mu$s. This is a great reduction for the inductor current ripple and hard to achieved in the conventional MPC unless the control cycle is reduced to 1/4 what it was. Therefore, it is concluded that the proposed method can effectively improve the performance of qZSI including the reduction of inductor current ripple and the output current THD.

## V. CONCLUSION

To overcome the drawback of the conventional MPC that causes large control error in the inductor current, the capacitor voltage, and the output current of the qZSI, this paper proposed combinative voltage vectors based MPC for the qZSI. Two different voltage vectors are applied in one control cycle for reducing the cost function value. Therefore, the qZSI using proposed method obtains low inductor current ripple and THD of output current over the conventional MPC. The improvement on the output current THD and the inductor current have the positive effect on the qZSI topology. On the one hand, obtaining low inductor current ripple indicates that small inductor can be used in the quasi Z-source inverter, and thus the volume and the cost of the qZSI can be reduced. On the other hand, the qZSI has better output performance. The experimental results verified that the effectiveness and the advantages of the proposed method.

## REFERENCES

[1] F. Z. Peng, "Z-source inverter," *IEEE Trans. Ind. Appl.*, vol. 39, no. 2, pp. 504–510, Mar./Apr. 2003.

[2] Y. He, H. Liu, W. Feng, and J. Li, "Novel cascaded Z-source neutral point clamped inverter," *Chin. J. Electron.*, vol. 25, no. 5, pp. 965–973, Sep. 2016.

[3] Y. He, Y. Xu, and J. Chen, "New space vector modulation strategies to reduce inductor current ripple of Z-source inverter," *IEEE Trans. Power Electron.*, vol. 33, no. 3, pp. 2643–2654, Mar. 2018.

[4] J. Anderson and F. Z. Peng, "Four quasi-Z-source inverters," in *Proc. IEEE Power Electron. Spec. Conf.*, Rhodes, Greece, Jun. 2008, pp. 2743–2749.

[5] O. Ellabban and H. Abu-Rub, "Z-source inverter: Topology improvements review," *IEEE Ind. Electron. Mag.*, vol. 10, no. 1, pp. 6–24, Mar. 2016.

[6] Y. He, Y. Xu, and J. Chen, "Improved space vector modulation of quasi Z-source inverter to suppress DC-link voltage sag," *IEEE Access*, vol. 7, pp. 66689–66702, 2019.

[7] X. Ding, Z. Qian, S. Yang, B. Cui, and F. Peng, "A PID control strategy for DC-link boost voltage in Z-source inverter," in *Proc. APEC*, Feb. 2007, pp. 1145–1148.

[8] X. Ding, Z. Qian, S. Yang, B. Cui, and F. Peng, "A direct peak DC-link boost voltage control strategy in Z-source inverter," in *Proc. APEC*, Feb. 2007, pp. 648–653.
[9] O. Ellabban, J. Van Mierlo, and P. Lataire, "A DSP-based dual-loop peak DC-link voltage control strategy of the Z-source inverter," *IEEE Trans. Power Electron.*, vol. 27, no. 9, pp. 4088–4097, Sep. 2012.
[10] Y. P. Siwakoti, F. Z. Peng, F. Blaabjerg, P. C. Loh, G. E. Town, and S. Yang, "Impedance-source networks for electric power conversion Part II: Review of control and modulation techniques," *IEEE Trans. Power Electron.*, vol. 30, no. 4, pp. 1887–1906, Apr. 2015.
[11] S. Bayhan, H. Abu-Rub, and R. S. Balog, "Model predictive control of quasi-Z-source four-leg inverter," *IEEE Trans. Ind. Electron.*, vol. 63, no. 7, pp. 4506–4516, Jul. 2016.
[12] H. Wu, K. Huang, W. Lv, X. Mo, and S. Huang, "DC-link voltage control strategy of Z-source inverter for high-speed permanent magnet motor," *IET Electr. Power Appl.*, vol. 14, no. 5, pp. 911–920, May 2020.
[13] S. Xiao, X. Gu, Z. Wang, T. Shi, and C. Xia, "A novel variable DC-link voltage control method for PMSM driven by a quasi-Z-source inverter," *IEEE Trans. Power Electron.*, vol. 35, no. 4, pp. 3878–3890, Apr. 2020.
[14] P. Karamanakos, T. Geyer, N. Oikonomou, F. D. Kieferndorf, and S. Manias, "Direct model predictive control: A review of strategies that achieve long prediction intervals for power electronics," *IEEE Ind. Electron. Mag.*, vol. 8, no. 1, pp. 32–43, Mar. 2014.
[15] R. S. Dastjerdi, M. A. Abbasian, H. Saghafi, and M. H. Vafaie, "Performance improvement of permanent-magnet synchronous motor using a new deadbeat-direct current controller," *IEEE Trans. Power Electron.*, vol. 34, no. 4, pp. 3530–3543, Apr. 2019.
[16] M. Mamdouh and M. A. Abido, "Efficient predictive torque control for induction motor drive," *IEEE Trans. Ind. Electron.*, vol. 66, no. 9, pp. 6757–6767, Sep. 2019.
[17] S. Vazquez, J. Rodriguez, M. Rivera, L. G. Franquelo, and M. Norambuena, "Model predictive control for power converters and drives: Advances and trends," *IEEE Trans. Ind. Electron.*, vol. 64, no. 2, pp. 935–947, Feb. 2017.
[18] S. Vazquez, J. I. Leon, L. G. Franquelo, J. Rodriguez, H. A. Young, A. Marquez, and P. Zanchetta, "Model predictive control: A review of its applications in power electronics," *IEEE Ind. Electron. Mag.*, vol. 8, no. 1, pp. 16–31, Mar. 2014.
[19] Y. Liu, H. Abu-Rub, Y. Xue, and F. Tao, "A discrete-time average model-based predictive control for a quasi-Z-source inverter," *IEEE Trans. Ind. Electron.*, vol. 65, no. 8, pp. 6044–6054, Aug. 2018.
[20] M. Mosa, R. S. Balog, and H. Abu-Rub, "High performance predictive control of quasi impedance source inverter," *IEEE Trans. Power Electron.*, vol. 32, no. 4, pp. 3251–3261, Apr. 2017.
[21] X. Zhang and Y. He, "Direct voltage-selection based model predictive direct speed control for PMSM drives without weighting factor," *IEEE Trans. Power Electron.*, vol. 34, no. 8, pp. 7838–7851, Aug. 2019.
[22] M. Norambuena, J. Rodriguez, Z. Zhang, F. Wang, C. Garcia, and R. Kennel, "A very simple strategy for high-quality performance of AC machines using model predictive control," *IEEE Trans. Power Electron.*, vol. 34, no. 1, pp. 749–800, Jan. 2019.
[23] Y. Zhang, Y. Peng, and H. Yang, "Performance improvement of two-vectors-based model predictive control of PWM rectifier," *IEEE Trans. Power Electron.*, vol. 31, no. 8, pp. 6016–6030, Aug. 2016.
[24] P. Karamanakos, A. Ayad, and R. Kennel, "A variable switching point predictive current control strategy for quasi-Z-source inverters," *IEEE Trans. Ind. Appl.*, vol. 54, no. 2, pp. 1469–1479, Mar./Apr. 2018.
[25] A. Ayad, P. Karamanakos, and R. Kennel, "Direct model predictive current control strategy of quasi-Z-source inverters," *IEEE Trans. Power Electron.*, vol. 32, no. 7, pp. 5786–5801, Jul. 2017.
[26] Y. Xu, Y. He, and S. Li, "Logical operation-based model predictive control for quasi-Z-source inverter without weighting factor," *IEEE J. Emerg. Sel. Topics Power Electron.*, vol. 9, no. 1, pp. 1039–1051, Feb. 2021.
[27] R. O. Ramírez, J. R. Espinoza, C. R. Baier, M. Rivera, F. Villarroel, J. I. Guzman, and P. E. Melin, "Finite-state model predictive control with integral action applied to a single-phase Z-source inverter," *IEEE J. Emerg. Sel. Topics Power Electron.*, vol. 7, no. 1, pp. 228–239, Mar. 2019.

**YUHAO XU** was born in Shaanxi, China, in 1990. He received the B.S. degree in automation and the M.S. degree in control theory and control engineering from Xi'an Polytechnic University, Xi'an, China, in 2012 and 2015, respectively, and the Ph.D. degree in electrical engineering from Northwestern Polytechnical University, Xi'an, in 2021.

He is currently a Lecturer with the School of Electronics Engineering, Xi'an Aeronautical University, Xi'an. His research interests include motor drives and power electronics control technologies, in particular model predictive control techniques.

**HAIFENG XIAO** was born in Ankang, Shaanxi, China, in 1978. He received the B.S. degree in automation and the M.S. degree in detection technology and automation device from Xi'an Polytechnic University, Xi'an, China, in 2003 and 2007, respectively, and the Ph.D. degree in armament science and technology from Northwestern Polytechnical University, Xi'an, in 2016.

He is currently a Full Professor with the School of Electronics Engineering, Xi'an Aeronautical University, Xi'an. Since 2020, he has been the Associate Dean of the School of Electronics Engineering, Xi'an Aeronautical University. His research interests include electrical machines, power electronics, and their control systems.